Chemical Science

ROYAL SOCIETY OF CHEMISTRY

EDGE ARTICLE

View Article Online
View Journal | View Issue

Cite this: *Chem. Sci.*, 2025, **16**, 9913

All publication charges for this article have been paid for by the Royal Society of Chemistry

Received 21st February 2025
Accepted 26th April 2025

DOI: 10.1039/d5sc01380a

rsc.li/chemical-science

Dynamic and interconnected influence of dissolved iron on the performance of alkaline water electrolysis†

Fubiao Di,‡[a] Cong Chen,‡[a] Junxia Shen,[a] Zhihe Wei,[b] Wen Dong,[a] Yang Peng,[b] Ronglei Fan,*[a] Mingrong Shen*[a] and Pierre-Yves Olu*[c]

Dissolved iron (Fe) species is an intriguing player in the overall alkaline water electrolysis (AWE) system, considered both as a poison that needs to be avoided and as a precursor for enhancing the water splitting activity. Here, we unveil the intricate mechanisms governing the Fe influence on practical AWE systems, by measuring the dynamic changes in cell voltage and overpotential of hydrogen evolution reaction (HER) and oxygen evolution reaction (OER). The dissolved Fe will deposit on the cathode, which significantly enhances the HER activity of bare Ni mesh (BN) while showing negligible impact on the porous RANEY® Ni mesh (RN). The dissolved Fe will also improve the OER activity of the BN by a mechanism based on an equilibrium between leaching and incorporation of Fe onto the oxide layer of the anode. The continuous deposition of Fe on the cathode will gradually deplete the electrolyte of dissolved Fe, which will in turn push the anode surface equilibrium towards low density of active Fe sites thus to a decrease of OER activity. Inspired by the above results, by optimizing the addition of Fe(III) salt into the system, an impressively low cell voltage of 1.95 V for a water splitting current density of 0.4 A cm^{-2} was achieved for a simple, cheap and robust BN cathode//BN anode zero-gap assembly. This performance is equivalent to a power consumption around 19.3% lower compared to the system without Fe(III) addition.

Introduction

Global hydrogen gas production reached around 95 million tonnes in 2022. This H_2 was overwhelmingly produced by fossil fuels (natural gas and coal) and only 0.1% of the H_2 was produced from electrolysis of water.[1] Based on the International Energy Agency (IEA) estimation of announced industrial projects, around 14 million tonnes of H_2 could be produced from water electrolysis in 2030, which would correspond to 160 GW newly installed electrolysis capacity. Around 60% of the industrial electrolyzers installed are so-called alkaline water electrolyzers (AWE), which is considered as the most mature technology.[2–4] The AWE system is usually fed with around 30 wt% KOH electrolyte and is operated between 60 and 90 °C. The most simple electrolyzer designs use bare nickel electrodes and chemically-treated polyphenylene sulfide (PPS) diaphragm as a separator in the cell.[5] A viable way to improve the water-splitting efficiency of the AWE is to use activated electrodes with more effective active sites. For the cathode, a widely used activated type for enhanced hydrogen evolution reaction (HER) activity is the RANEY® Ni coating, produced by selectively leaching Al or Zn from a precursor (NiAl or NiZn) alloy.[6–8] For the anode, materials based on a mixture of Ni and Fe are commonly used to improve the oxygen evolution reaction (OER).[9–12]

Iron (Fe) species can be present in the electrolyte of the AWE during operation, coming mainly from the corrosion product of the balance of stack or continuously added with the make-up water.[13–15] Considering purely the activity of the electrodes, the presence of Fe in the electrolyte seems to be beneficial to both the HER and OER activity, when the electrodes are based on Ni active material and not platinum group metals (PGM).[16–18] Demnitz *et al.* showed in laboratory-scale cell and industrial operating conditions (30 wt% KOH, 90 °C) that Fe addition to the electrolyte can simultaneously promote the HER and OER of bare Ni electrodes by lowering the overpotential of each reaction by at least 100 mV at 0.8 A cm^{-2}. The improvement of HER activity was attributed to the formation of Fe dendrite layers

[a]*School of Physical Science and Technology, Jiangsu Key Laboratory of Frontier Material Physics and Devices, Collaborative Innovation Center of Suzhou Nano Science and Technology, Soochow University, 1 Shizi Street, Suzhou, 215006, China. E-mail: rlfan@suda.edu.cn; mrshen@suda.edu.cn*

[b]*Soochow Institute of Energy and Material Innovations, College of Energy, Provincial Key Laboratory for Advanced Carbon Materials and Wearable Energy Technologies, Soochow University, 688 Moye Road, Suzhou, 215006, China*

[c]*John Cockerill Hydrogen S. A, 1 Rue Jean Potier, Seraing, 4100, Belgium. E-mail: pierre-yves.olu@johncockerill.com*

† Electronic supplementary information (ESI) available. See DOI: https://doi.org/10.1039/d5sc01380a

‡ Both authors contributed equally to this manuscript.

that form on the cathode surface, while the improvement in OER was credited to the formation of thin layers of mixed Ni/Fe oxyhydroxides on the anode surface.[19] In the present work, we started from this base and settled to investigate: (i) what is the effect of Fe on an advanced porous RANEY® nickel cathode instead of simple bare nickel cathode, and (ii) what are the dynamics of the whole zero-gap cell assembly, knowing that both the cathode and anode interplay with Fe dissolved in a common electrolyte. To entangle this interplay of Fe-effect on HER and OER, we mounted laboratory-scale zero-gap assembly with operating conditions close to real industrial AWE (30 wt% KOH, 60 °C, PPS diaphragm). Two different materials are used as cathodes, the bare nickel mesh (BN) and the porous RANEY® nickel mesh (RN), and BN is used as anode, so two different electrolyzers are formed (BN//BN, RN//BN). Then, by adding a certain concentration of Fe(III) salt in the electrolyte and monitoring the dynamic changes in cell voltage and overpotential of cathode and anode simultaneously at a constant 0.4 A cm^{-2} during 48 h of operation, we could investigate in fine details how the presence of Fe affects the overall performance of the AWE system.

Results and discussion

Fig. 1a shows the cell voltages of BN//BN and RN//BN electrolyzers in purified KOH with and without 150 μM Fe(III) salt. The benefit of using a porous RN cathode is obvious in an environment matching industrial AWE operating conditions but free of dissolved Fe in the electrolyte. The use of commercial porous RN cathode enables around 270 mV decrease of the cell voltage at 0.4 A cm^{-2} current density after 48 h of relatively stable operation. It is a substantial improvement in equipment efficiency worth paying additional costs for the cathode component. The use of porous RN cathode would improve the power efficiency of the AWE system by 11.1% for the same rate of H_2 generated (the detailed calculation process can be found in ESI†).

The superiority of porous RN cathode is not so clear anymore when dissolved Fe comes into play. When 150 μM of Fe(III) is added to the electrolyte prior to the experiment, the cell voltages significantly decrease whatever the type of cathode used. The impact of dissolved Fe is relatively more important when BN is used as the cathode instead of porous RN. Surprisingly, the performance of the simple BN//BN cell assembly shows similar performance as the more advanced RN//BN cell assembly around 3 h at the beginning of the experiment (Fig. 1a). The performance of BN//BN assembly is however not stable and progressively decays after the experiment exceeds 4 h duration. The initial addition of 150 μM Fe(III) salt decreases the BN//BN cell voltage by 410 mV, *i.e.* a transitory improvement of AWE power efficiency of 16.8%. The simple addition of unexpensive Fe(III) salts had, for a short duration, 1.5 times more beneficial impact on the power efficiency of the cell compared to the cathode with porous RANEY® Ni coating. When porous RN is used as cathode, the beneficial effect of 150 μM Fe(III) salt addition still occurs, however with relatively less impact but also slower decay than the BN cathode. The overpotential gain for RN//BN assembly is around 270 mV after Fe(III) salt addition, *i.e.* a possible 12.4% of better AWE power efficiency. The total cell voltage of a 2-electrodes assembly is dependent of the individual overpotentials of the 2 electrodes, it is not possible from Fig. 1a only to distinguish between cathodic and anodic contribution on the cell behavior described above. A reference electrode was therefore inserted at selected moments during the experiment which enabled to follow the individual the behaviors of the anode and the 2 types of cathodes (see Fig. S1† for a scheme of the experimental setup).

The performance of porous RN cathode is not impacted by the presence of dissolved Fe. As shown in Fig. 1b, for both purified KOH and Fe(III)-added KOH electrolytes, the porous RN cathode progressively gets better, reaching an apparent stable HER overpotential of 310 mV. This progressive performance enhancement is attributed to slow Al leaching and crystallographic phase rearrangement of the Ni_xAl_y phases of the RANEY® alloy, possibly increasing both its porosity and intrinsic activity.[6,20–22] On the other hand, the performance of BN cathode is significantly enhanced by the presence of dissolved Fe. As shown in Fig. 1b, the HER overpotential of the BN

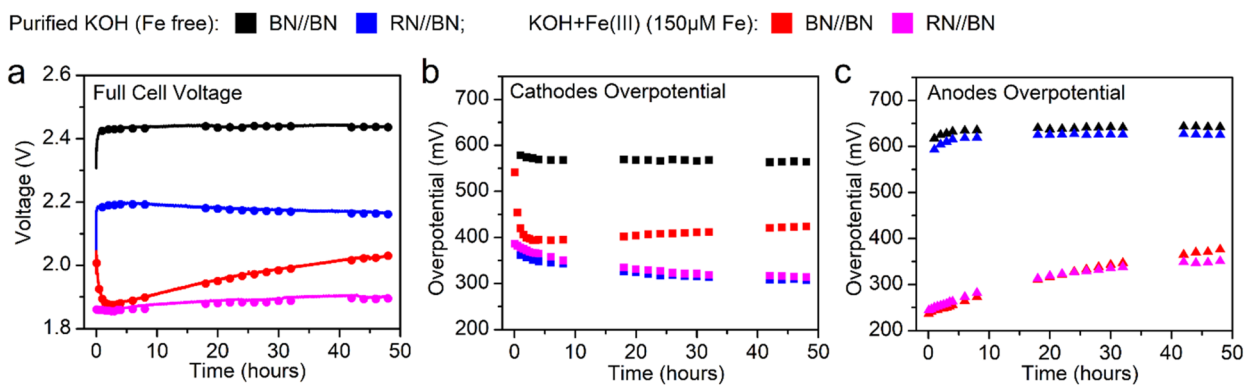

Fig. 1 (a) Cell voltages, (b) cathode overpotentials (taken against 0 V *vs.* RHE) and (c) anode overpotentials (taken against 1.23 V *vs.* RHE) of BN//BN and RN//BN electrolyzers over time in purified 30 wt% KOH with and without 150 μM Fe(III) salt. The dots correspond to the moment when reference electrode is inserted in the electrolyzer for individual overpotential measurements. BN//BN: the assembly with bare nickel mesh as cathode and bare nickel mesh as anode; RN//BN: the assembly with porous RANEY® nickel as cathode and bare nickel as anode.

cathode first decreases by 150 mV after 3 h of constant HER in Fe-containing electrolyte. After $t = 3$ h, the performance of the BN cathode in Fe-containing KOH slowly decays to reach an overpotential of 420 mV after 48 h at 0.4 A cm^{-2}. After 48 h of operation and reaching apparent stability, the gain of using commercial porous RN cathode in a Fe-free environment is around 250 mV while it is only 110 mV when Fe(III) salt was initially added to the KOH electrolyte.

The performance of the BN anode is even more significantly enhanced by the presence of dissolved Fe. As shown in Fig. 1c, adding Fe(III) salt in the KOH initially improves the OER overpotential of the BN anode by around 360 mV. This beneficial effect of Fe(III) salt initial addition is however not stable, the anode performance progressively decays with time. After 48 h of constant 0.4 A cm^{-2} current density, the gain in OER overpotential is reduced to around 270 mV which is still a significant effect. The individual behavior of the BN anode does not depend on the type of cathode used in the cell assembly, which reinforces the confidence in the reproducibility of this experiment. Looking at the individual potentials of the electrodes enable to conclude that initial Fe(III) salt addition to the electrolyte enhances both the performance of BN both as anode and cathode although this enhancement is not stable, while porous RN cathode is not affected. Now, these observations do not explain why the cathodic and anodic performance are (or are not) affected by dissolved Fe. To further investigate if the change of performance is due to an increase of the electrode active area and/or by a change of catalytic intrinsic activity, one needs to look at the HER or OER activities normalized either to the geometric surface or to the electrochemically active surface area.

The linear sweep voltammetry (LSV) curves of various electrodes with 95% IR correction performed at the beginning ($t =$ 0 h) and the end of experiment ($t = 48$ h) logically show the same trends as previously developed when normalized to the 1×1 cm^2 electrodes meshes geometric area (Fig. 2a, d and g). The Nyquist plots and solution resistances of various electrodes were shown in Fig. S2 and Table S1.† That is to say: (i) progressive beneficial effect of the Fe(III) addition for the HER performance of the BN cathode; (ii) no beneficial effect of the Fe(III) addition for the HER performance of the porous RN cathode; (iii) progressive HER improvement of the porous RN cathode with and without Fe(III) added; (iv) immediate beneficial effect of the Fe(III) addition for the OER performance of the BN anode but (v) progressive decrease of this OER beneficial effect. In order to get further insights on the phenomenon behind these observations, the electrochemically active surface area (ECSA) of these electrodes were also measured at $t = 0$ h and $t = 48$ h. The ECSA was tested by reading the capacitive current of the electrodes upon potential cycling at various sweep rates within a potential window without faradaic current (Fig. S3–S5†). The normalization of the LSV curves to the as-measured ECSA lead to a new angle of observation for the HER and OER activities of these electrodes..

The HER improvement of the BN cathode is completely attributed to the progressive increase of surface area thanks to progressive electrodeposition of Fe on the BN surface. Indeed, as shown in Fig. 2b, the ECSA normalized HER activity is actually the worst for the BN cathode at $t = 48$ h with initial addition of Fe(III), while this electrode shows the best absolute HER activity (Fig. 2a). The porous Fe/Fe (hydr)oxide deposited onto the Ni surface after 48 h operation is confirmed by scanning electron microscope (SEM) (Fig. 2c and S6†), energy dispersive X-ray (EDX) (Fig. S7†), Raman (Fig. S8†) and X-ray photoelectron spectroscopy measurement (Fig. S9†). This observation is in agreement with past studies concluding that the intrinsic HER activity of Fe is slightly lower than Ni in alkaline media.[23,24] Therefore, the ECSA normalized HER activity of an electrode covered by porous Fe cannot be higher than the initial Ni, even if the progressive increase of HER active site by Fe deposition is sufficient to significantly improve the absolute HER activity of the BN cathode. Similar cathodic behavior was observed on perforated Ni plate in flow cell with Fe(III) salt addition by Demnitz *et al.*[19] Moreover, no other peaks corresponding to Fe species can be found from XRD patterns for BN cathode and RN cathode after Fe deposition, indicating the amorphous property (Fig. S10†).

On the other hand, for porous RN cathode, the presence of Fe is negligeable for the HER activity and the progressive improvement of HER activity is a combination of increased ECSA and better intrinsic activity (Fig. 2e). This is attributed to the further leaching of Al element from the Ni_xAl_y alloy of the RANEY® nickel during immersion in hot 30 wt% KOH, which can have the dual effect of increasing the porosity thus the ECSA and the intrinsic HER activity by changing the Ni/Al ratio of the RANEY® coating.[20–22,25] Deposition of Fe/Fe (hydr)oxide onto the porous RN surface is nevertheless confirmed by SEM observation (Fig. 2f and S11†), EDX, Raman and XPS measurements (Fig. S12–S14†). However, the SEM images show that the deposition of the Fe does not block the initial porous RANEY® layer, explaining the negligeable influence of the Fe on the HER performance of porous RN cathode.

Contrary to the HER, for the OER the improvement of the BN anode with Fe(III) salt addition is not due to an increase of the active surface, but to an increase of the intrinsic OER activity, as shown in Fig. 2h. Fe (hydr)oxide is detected on the surface of the BN anode at $t = 48$ h (Fig. S15†). However, Fe can hardly be detected in the initial BN (Fig. S16†). And no quantitative Fe layer deposition is observed by SEM image (Fig. 2i). The increase of intrinsic OER activity is attributed to a dynamic equilibrium for the incorporation of the dissolved Fe species into the Ni oxide layer anode (typical nanosheets can be seen in Fig. S17†). The presence of Fe into the Ni oxide layer creates new sites with high activity for the OER, without necessarily increasing the ECSA of the electrode. This phenomenon, explaining the immediate improvement of OER activity when Fe(III) salt is initially added to the electrolyte, which could be ascribed to the consumption of Fe ions in the electrolyte, in line with the most recent studies on this topic.[16,26–29] To prove this point, we added the same amount of Fe ions into the electrolyte after 48 h operation, the activity of BN anode is restored again (Fig. S18†). However, it is clear that in our experiment, the beneficial effect of Fe is not stable and progressively weakens during the 48 h water splitting experiment[30] As the presence of dissolved Fe is now demonstrated to have a major role in

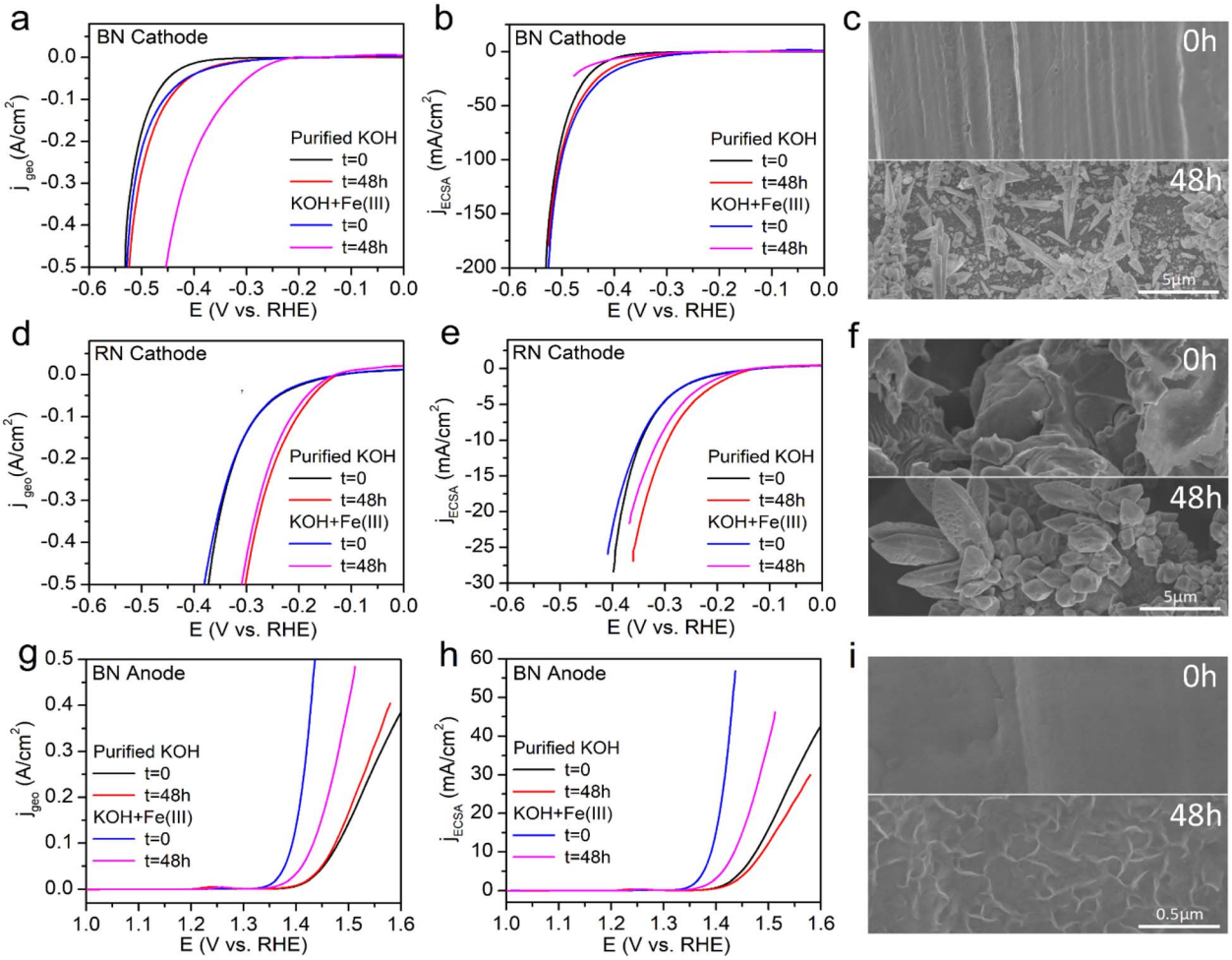

Fig. 2 (a, d and g) Geometric area normalized LSV curves with 95% IR correction, (b, e and h) ECSA normalized LSV curves, and (c, f and i) SEM images of various electrodes before ($t = 0$ h) and after ($t = 48$ h) constant current test in purified 30 wt% KOH with and without 150 μM Fe(III) salt: (a–c) BN cathode; (d–f) RN cathode; (g–i) BN anode.

intrinsic OER activity, in the following we will investigate about the dynamic change of Fe species during the experiment.

The dynamic performances of the present results are attributed to the change in the concentration of dissolved Fe in the system. As shown in Fig. 3a, the Fe concentration after the 48 h of constant current experiment is decreased to a low value of 0.42 mg L^{-1} while the initial Fe concentration of this KOH electrolyte before operation was 8.38 mg L^{-1} (*i.e.* 150 μM of Fe(III) as initially targeted). This final Fe concentration after 48 h is not far from the measured Fe concentration of the KOH electrolyte initially purified (0.2 mg L^{-1}). The electrolyte is therefore being gradually depleted in dissolved Fe during the constant electrolysis condition. This is not surprising, as quantitative Fe deposits were observed on the cathodes (Fig. 2c and S6†). The gradual decrease of dissolved Fe explains why, after a first immediate OER activity improvement with initial Fe(III) addition, the OER performances of the BN anode gradually deteriorate (Fig. 1c). The underlying mechanism is proposed to be an equilibrium between Fe incorporation into the oxide layer on anodic BN, and a leaching of these Fe OER active sites to the electrolyte upon corrosive OER conditions. In this mechanism, the density of OER active sites related to Fe incorporated to the oxide layer is dependent on the concentration of Fe dissolved in the nearby electrolyte, in agreement with past studies about Fe effect on OER.[31,32] However, the cathode is continuously consuming dissolved Fe by electro-deposition reduction reaction to its surface. The concentration of dissolved Fe is therefore gradually decreasing, leading to a gradual degradation of the anodic OER performance. Dissolved Fe influence both the cathode and anode but with two distinct mechanisms. For the anode, the beneficial presence of Fe on the oxide layer is proposed as incorporation/leaching equilibrium, meaning that after a first near immediate consumption of dissolved Fe on the initially Fe-free Ni oxide anodic surface, the equilibrium is stable on the condition that dissolved Fe concentration in the nearby electrolyte stays constant. For the cathode, the electro-deposition of Fe on the surface (which can be beneficial, negligeable or detrimental for the HER performance depending on the initial state of the cathode surface) is continuously consuming dissolved Fe in the electrolyte, breaking the equilibrium on the anode side and explaining the gradual degradation of the OER performances. One can

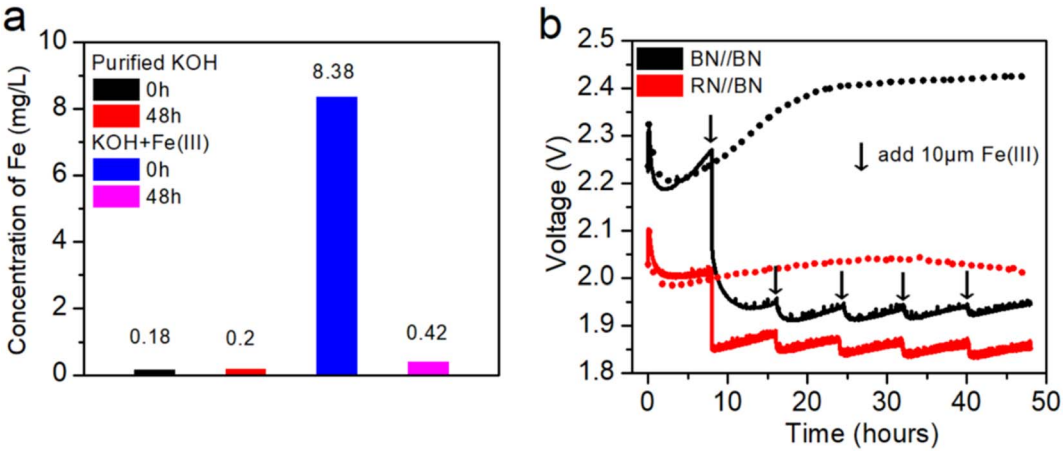

Fig. 3 (a) Concentration of dissolved Fe for the BN//BN cell assembly in purified 30 wt% KOH with and without 150 μM Fe(III) salt at $t = 0$ h and $t =$ 48 h, measured by ICP-OES. (b) Time evolution of the cell voltage (without any prior purification nor initial addition of Fe(III) salt) for BN//BN (in black) and RN//BN (in red). Periodical addition of 10 μM Fe(III) salt into the electrolyte illustrated by the vertical black arrows on the figure. Reference experiments without any addition of Fe(III) salt in dotted line.

therefore understand that a system composed of a BN anode and a BN cathode sharing a common KOH electrolyte with a fixed initial concentration of dissolved Fe cannot output stable performance unless there is an outside continuous addition of dissolved Fe to maintain a stable Fe concentration in the electrolyte.

Periodic addition of Fe(III) salt in the electrolyte can indeed sustain the beneficial effect of the presence of dissolved Fe during the 48 h of constant water splitting experiment. As shown in Fig. 3b, addition of 10 μM of Fe(III) salt every 8 h enables staying around 1.93 V cell voltage for the simple BN//BN system at 0.4 A cm^{-2} and 60 °C, which is a remarkable performance at this condition for such simple electrodes. By periodically adding small amount of Fe(III) salt instead of one big initial addition, the beneficial effect of dissolved Fe on the OER activity of the anode can be valorized for a longer duration due to both kinetics of cathodic and anodic Fe-related mechanisms introduced above in the present study. At the end of the 48 h constant current experiment, the BN//BN cell gained around 0.47 V in performance when using periodic addition of Fe(III), *i.e.* a lower power consumption of around 19.3% or in other words a significant efficiency gain of 1.12 kW h Nm^{-3} of H_2. Using a more advanced cathode as commercial porous RN still has benefits compared to bare BN even when Fe(III) is periodically added to the electrolyte. As shown in Fig. 3b, in our experimental conditions after 48 h of constant current with periodic addition of Fe(III), the use of porous RN cathode leads to around 0.09 V lower cell voltage compared to simple BN cathode (an efficiency gain of 0.22 kW h Nm^{-3} of H_2). The detailed dynamic changes in overpotentials of anode and cathode for BN//BN and RN//BN electrolyzer are shown in Fig. S19.† Considering that the HER activity of the porous RN cathode is progressively getting better with operation time (for reasons discussed earlier in the present study), the benefits of using porous RN cathode over simple BN cathode could continue to increase over time. Note that in Fig. 3b, the experiments were performed on a 30 wt% KOH electrolyte which was not purified and without any initial Fe(III) addition (which was the case in Fig. 1a), therefore initially containing a dissolved Fe concentration in between these 2 extremes initial conditions and explaining why the voltages of the zero-gap cells for the first 8 h in Fig. 3b lie between the cell voltages of Fig. 1a.

The present study was performed on small scale of 1×1 cm^2 and short duration of 48 h. Nevertheless, the results discussed above are clear enough to risk extrapolating the discussion on much larger industrial AWE systems. The management of the Fe content in the system appears to be critical. Based on our findings, a simple low-capital AWE system with non-activated electrodes (BN as both cathode and anode) could, if dissolved Fe concentration in the system is always maintained above around 0.5 mg L^{-1}, sustain medium current densities (around 0.4 A cm^{-2}) at competitive power consumption. This would be a clear advancement of the present industrial proposition, but would this strategy be stable? One can understand that it is not viable as is. Indeed, continuously added Fe in the system will continuously deposit on the cathode, which is bound to create serious issues for the equipment. The continuous deposition of Fe on the BN cathode can even progressively soften the roughness of the deposit, therefore decreasing the porosity initially formed and thus deteriorate the beneficial HER improvement. An ideal strategy could be to separate the catholyte and the anolyte: (i) keep the catholyte at low concentration of Fe to avoid continuous deposition, while using an activated cathode (such as porous Ni type) for high HER activity; (ii) keep the anolyte at high concentration of Fe and use simple BN anode to benefit from the improvement of OER activity at low cost. Considering the present findings, this kind of practical research has potential to improve the attractiveness of AWE industrial proposition.

Our findings also shed further light on why it is so difficult to reliably benchmark components of the AWE system like the electrodes and diaphragms.[33,34] Electrode surfaces change during the experiment, and this change is linked to numerous

interconnected parameters. How the testing equipment is designed: can the balance of stack release Fe or other species, how the system is heating, or the components are electrically connected and mounted against each other. From an industrial perspective, the best benchmarking is the one closest to the operating conditions on site, but every AWE manufacturer has its own operating parameters, which seem like an unsolvable dilemma. For the electrodes (cathodes and anodes), our benchmarking proposition is a follow: to test the electrodes in the 2 extremes conditions "Fe-free" and "continuous addition of Fe", using around 30 wt% KOH, under at least 60 °C for at least 24 h of continuous operation to the targeted current density. This way, one can show if the electrodes are sensitive to Fe, in a beneficial way (for instance the BN anode and cathode), in a detrimental way (possibly the noble metal based cathodes) or not sensitive (for instance porous RN cathode).

Conclusions

In summary, we demonstrated on lab-scale zero-gap cell assembly the intricate mechanisms governing the Fe influence on practical AWE systems. The iron dissolved in the electrolyte is electrodeposited on the cathode forming a porous iron-based layer. If the cathode is initially of low active surface area like a simple BN, this phenomenon will significantly enhance the HER activity. However, if the cathode has a large initial active surface like porous RN, the deposition of iron does not significantly impact the HER activity. The dissolved Fe will also improve the OER activity of the BN anode by another mechanism based on an equilibrium between leaching and incorporation of Fe onto the oxide layer of the anode. The cathodic and anodic mechanisms, connected *via* a common electrolyte, are antagonists. The continuous deposition of Fe on the cathode will gradually deplete the electrolyte of dissolved Fe, which will in turn push the anode surface equilibrium towards low density of active Fe sites thus to a decrease of OER activity, creating by-design instability of the whole system performance. By continuously adding Fe(III) salt into the system, we reached remarkable performance of 1.95 V after 48 h of constant 0.4 A cm^{-2} current at 60 °C for simple, cheap and robust BN cathode//PPS diaphragm//BN anode zero-gap assembly. This performance is equivalent to a power consumption around 19.3% lower compared to the system without continuous Fe(III) addition. Conceptually, these findings also explain why benchmarking of AWE components is no easy task, and open the way to considering the dynamic state of the electrolyte as a part of the practical "electrode" element.

Data availability

The data supporting this article have been included as part of the ESI.†

Author contributions

Fubiao Di: conceptualization, methodology, investigation, data curation, writing – original draft. Cong Chen: conceptualization, methodology, data curation, writing – review & editing. Junxia Shen: formal analysis, investigation. Zhihe Wei: formal analysis, investigation. Wen Dong: formal analysis, investigation. Yang Peng: methodology, visualization. Ronglei Fan: methodology, visualization, supervision, project administration, funding acquisition, writing – review & editing. Mingrong Shen: supervision, project administration, funding acquisition, writing – review & editing. Pierre-Yves Olu: formal analysis, investigation, methodology, visualization, writing – review & editing.

Conflicts of interest

There are no conflicts to declare.

Acknowledgements

This work was supported by National Natural Science Foundation of China (Grant No. 52002259, 52372216, and 52272228), and a key project of carbon peak carbon neutralization technology support from Suzhou Science and Technology Bureau (Grant No. ST202227).

References

1 IEA, *Global Hydrogen Review 2023*, 2025, Available at: **https://www.iea.org/reports/global-hydrogen-review-2023**.
2 C. T. Bowen, H. J. Davis, B. F. Henshaw, R. Lachance, R. L. LeRoy and R. Renaud, *Int. J. Hydrogen Energy*, 1984, **9**, 59–66.
3 K. Zeng and D. Zhang, *Prog. Energy Combust. Sci.*, 2010, **36**, 307–326.
4 F. Lehner and D. Hart, in *Electrochemical Power Sources: Fundamentals, Systems, and Applications*, ed. T. Smolinka and J. Garche, Elsevier, 2022, pp. 1–36, DOI: **10.1016/B978-0-12-819424-9.00008-2**.
5 S. Hu, B. Guo, S. Ding, F. Yang, J. Dang, B. Liu, J. Gu, J. Ma and M. Ouyang, *Appl. Energy*, 2022, **327**, 120099.
6 D. Chade, L. Berlouis, D. Infield, A. Cruden, P. T. Nielsen and T. Mathiesen, *Int. J. Hydrogen Energy*, 2013, **38**, 14380–14390.
7 J.-E. Kim, K.-K. Bae, C.-S. Park, S.-U. Jeong, K.-H. Baik, J.-W. Kim, K.-S. Kang, K.-B. Lee and Y.-H. Kim, *J. Ind. Eng. Chem.*, 2019, **70**, 160–168.
8 W. J. F. Gannon and C. W. Dunnill, *Electrochim. Acta*, 2019, **322**, 134687.
9 M. Chatenet, B. G. Pollet, D. R. Dekel, F. Dionigi, J. Deseure, P. Millet, R. D. Braatz, M. Z. Bazant, M. Eikerling, I. Staffell, P. Balcombe, Y. Shao-Horn and H. Schäfer, *Chem. Soc. Rev.*, 2022, **51**, 4583–4762.
10 L. Trotochaud, S. L. Young, J. K. Ranney and S. W. Boettcher, *J. Am. Chem. Soc.*, 2014, **136**, 6744–6753.
11 J. Zhao, J. J. Zhang, Z. Y. Li and X. H. Bu, *Small*, 2020, **16**, 2003916.
12 J.-F. Huang and W.-Z. Xie, *Chem. Sci.*, 2020, **11**, 6012–6019.
13 H. Becker, J. Murawski, D. V. Shinde, I. E. L. Stephens, G. Hinds and G. Smith, *Sustainable Energy Fuels*, 2023, **7**, 1565–1603.

14 R. Davalos Monteiro, J. van de Wetering, B. Krawczyk and D. L. Engelberg, *Met. Mater. Int.*, 2019, **26**, 630–640.
15 N. Todoroki and T. Wadayama, *Int. J. Hydrogen Energy*, 2022, **47**, 32753–32762.
16 A. Bukowski, P.-Y. Olu, A. Gering, M. Chatenet and A. Bonnefont, *Curr. Opin. Electrochem.*, 2024, **47**, 101568.
17 M. T. de Groot, *Curr. Opin. Chem. Eng.*, 2023, **42**, 100981.
18 Q. Kang, D. Lai, W. Tang, Q. Lu and F. Gao, *Chem. Sci.*, 2021, **12**, 3818–3835.
19 M. Demnitz, Y. M. Lamas, R. L. Garcia Barros, A. de Leeuw den Bouter, J. van der Schaaf and M. Theodorus de Groot, *iScience*, 2024, **27**, 108695.
20 F. Razmjooei, T. Liu, D. A. Azevedo, E. Hadjixenophontos, R. Reissner, G. Schiller, S. A. Ansar and K. A. Friedrich, *Sci. Rep.*, 2020, **10**, 10948.
21 Y. Zheng, Y. Jiao, A. Vasileff and S. Z. Qiao, *Angew. Chem., Int. Ed.*, 2018, **57**, 7568–7579.
22 S.-i. Tanaka, N. Hirose, T. Tanaki and Y. H. Ogata, *J. Electrochem. Soc.*, 2000, **147**, 2242.
23 M. Ďurovič, J. Hnát and K. Bouzek, *J. Power Sources*, 2021, **493**, 229708.
24 B. H. R. Suryanto, Y. Wang, R. K. Hocking, W. Adamson and C. Zhao, *Nat. Commun.*, 2019, **10**, 5599.
25 F. Devred, B. W. Hoffer, W. G. Sloof, P. J. Kooyman, A. D. van Langeveld and H. W. Zandbergen, *Appl. Catal., A*, 2003, **244**, 291–300.
26 I. Spanos, J. Masa, A. Zeradjanin and R. Schlögl, *Catal. Lett.*, 2020, **151**, 1843–1856.
27 S. Anantharaj, S. Kundu and S. Noda, *Nano Energy*, 2021, **80**, 105514.
28 Q. Zhang, W. Xiao, H. C. Fu, X. L. Li, J. L. Lei, H. Q. Luo and N. B. Li, *ACS Catal.*, 2023, **13**, 14975–14986.
29 Z. Wang and H. Xiao, *J. Am. Chem. Soc.*, 2024, **146**, 29540–29550.
30 R. Farhat, J. Dhainy and L. I. Halaoui, *ACS Catal.*, 2019, **10**, 20–35.
31 D. Y. Chung, P. P. Lopes, P. Farinazzo Bergamo Dias Martins, H. He, T. Kawaguchi, P. Zapol, H. You, D. Tripkovic, D. Strmcnik, Y. Zhu, S. Seifert, S. Lee, V. R. Stamenkovic and N. M. Markovic, *Nat. Energy*, 2020, **5**, 222–230.
32 D. Tyndall, M. J. Craig, L. Gannon, C. McGuinness, N. McEvoy, A. Roy, M. García-Melchor, M. P. Browne and V. Nicolosi, *J. Mater. Chem. A*, 2023, **11**, 4067–4077.
33 S. Appelhaus, L. Ritz, S.-V. Pape, F. Lohmann-Richters, M. R. Kraglund, J. O. Jensen, F. Massari, M. Boroomandnia, M. Romanò, J. Albers, C. Kubeil, C. Bernäcker, M. S. Lemcke, N. Menzel, G. Bender, B. Chen, S. Holdcroft, R. Delmelle, J. Proost, J. Hnát, P. Kauranen, V. Ruuskanen, T. Viinanen, M. Müller, T. Turek and M. Shviro, *Int. J. Hydrogen Energy*, 2024, **95**, 1004–1010.
34 N. Thissen, J. Hoffmann, S. Tigges, D. A. M. Vogel, J. J. Thoede, S. Khan, N. Schmitt, S. Heumann, B. J. M. Etzold and A. K. Mechler, *ChemElectroChem*, 2023, **11**, 202300432.